Acta Crystallographica Section F
**Structural Biology and Crystallization Communications**
ISSN 1744-3091

# Comparison of GFL–GFR$\alpha$ complexes: further evidence relating GFL bend angle to RET signalling

**Vimal Parkash[a] and Adrian Goldman[a,b]***

[a]Institute of Biotechnology, University of Helsinki, Helsinki, Finland, and [b]Neuroscience Center, University of Helsinki, Helsinki, Finland

Correspondence e-mail: adrian.goldman@helsinki.fi

Received 14 January 2009
Accepted 11 May 2009

**PDB Reference:** GDNF–GFR$\alpha$1 complex, 3fub, r3fubsf.

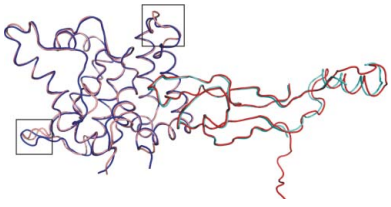



Glial cell line-derived neurotrophic factor (GDNF) activates the receptor tyrosine kinase RET by binding to the GDNF-family receptor $\alpha$1 (GFR$\alpha$1) and forming the $GDNF_2$–$GFR\alpha1_2$–$RET_2$ heterohexamer complex. A previous crystal structure of the $GDNF_2$–$GFR\alpha1_2$ complex (PDB code 2v5e) suggested that differences in signalling in GDNF-family ligand (GFL) complexes might arise from differences in the bend angle between the two monomers in the GFL homodimer. Here, a 2.35 Å resolution structure of the $GDNF_2$–$GFR\alpha1_2$ complex crystallized with new cell dimensions is reported. The structure was refined to a final $R$ factor of 22.5% ($R_{free}$ = 28%). The structures of both biological tetrameric complexes in the asymmetric unit are very similar to 2v5e and different from the artemin–GFR$\alpha$3 structure, even though there is a small change in the structure of the GDNF. By comparison of all known GDNF and artemin structures, it is concluded that GDNF is more bent and more flexible than artemin and that this may be related to RET signalling. Comparisons also suggest that the differences between artemin and GDNF arise from the increased curvature of the artemin 'fingers', which both increases the buried surface area in the monomer–monomer interface and changes the inter-monomer bend angle. From sequence comparison, it is suggested that neuturin (the second GFL) adopts an artemin-like conformation, while persephin has a different conformation to the other three.

## 1. Introduction

Glial cell line-derived neurotrophic factor (GDNF) has a broad range of functions as a survival factor and a regulator for central and peripheral neurons, as well as being a morphogenic factor in kidney and spermatogonia development (Airaksinen & Saarma, 2002). The GDNF family of ligands (GFLs) consists of four neurotrophic factors: GDNF, neurturin (NRTN; Kotzbauer *et al.*, 1996), artemin (ARTN; Baloh *et al.*, 1998) and persephin (PSPN; Milbrandt *et al.*, 1998). The crystal structure of GDNF is a covalently linked symmetric homodimer in which monomers composed of two $\beta$-stranded 'fingers' and a helix, called the heel, are tied together by a 'cystine knot' (Fig. 1*a*; PDB code 1agq; Eigenbrot & Gerber, 1997). The GDNF crystal contains two independent covalent homodimers that differ in the relative hinge angle between the fingers and the heel within their respective monomers (Eigenbrot & Gerber, 1997).

All GFLs signal through a two-receptor system. The first receptor, GDNF-family receptor $\alpha$ (GFR$\alpha$), which is glycosyl-phosphatidyl-inositol anchored to the cell surface, is required for ligand binding. The GFL homodimer binds two molecules of GFR$\alpha$ and the binding is specific: GDNF binds GFR$\alpha$1, NRTN binds GFR$\alpha$2, ARTN binds GFR$\alpha$3 and PSPN binds GFR$\alpha$4 (Fig. 2; Airaksinen & Saarma, 2002). In addition, GDNF, NRTN and ARTN show weak crosstalk with GFR$\alpha$1 (Airaksinen *et al.*, 1999). GFR$\alpha$s have three homologous domains (D1, D2 and D3) and a C-terminal extension, except for GFR$\alpha$4, which lacks D1 (Fig. 2; Airaksinen *et al.*, 1999; Lindahl *et al.*,

2001). The second receptor, RET (REarranged during Transfection), is a common signalling receptor for all the GFLs (Airaksinen *et al.*, 1999). RET has four cadherin-like domains (CLDs; CLD1–4) and a cysteine-rich domain (CRD) in its extracellular region, which is followed by a transmembrane segment and two tyrosine kinase domains in its intracellular region (Fig. 2). RET activation requires the formation of a heterohexameric complex $GDNF_2$–$GFR\alpha1_2$–$RET_2$, which leads to transphosphorylation and subsequent intracellular signalling (Airaksinen *et al.*, 1999).

The structures of the $GDNF_2$–$GFR\alpha1_2$ (PDB code 2v5e) and $ARTN_2$–$GFR\alpha3_2$ (PDB code 2gh0) complexes (Wang *et al.*, 2006; Parkash *et al.*, 2008), together with previous studies (Scott & Ibáñez, 2001; Leppänen *et al.*, 2004), established that GFR$\alpha$ D2 binds the GFL ligand fingers. The crystal structure 2v5e (Parkash *et al.*, 2008) contained only the two binding domains in GFR$\alpha$1 (domains 2 and 3; D23), each composed of a bundle of five $\alpha$-helices: 'the triangular $\alpha$-spiral fold' (Leppänen *et al.*, 2004). Mutagenesis, structural and biochemical studies (Eketjäll *et al.*, 1999; Wang *et al.*, 2006; Parkash *et al.*, 2008) showed that the $ARTN_2$–$GFR\alpha3_2$ and $GDNF_2$–$GFR\alpha1_2$ structures differ at the interface between the GFL and the GFR$\alpha$ because of the changes $Ile175^{GFR\alpha1}\rightarrow Gly^{GFR\alpha3}$, $Asn162^{GFR\alpha1}\rightarrow Thr^{GFR\alpha3}$, $Tyr120^{GDNF}\rightarrow Trp^{ARTN}$ and $Leu114^{GDNF}\rightarrow Met^{ARTN}$. In addition, enzyme-linked immunosorbent assays of RET phosphorylation suggested that the GFR$\alpha$1 residues Arg190, Lys194, Arg197, Gln198, Lys202, Arg257, Arg259, Glu323 and Asp324 in domains D2 and D3 interact with RET (Parkash *et al.*, 2008). In the GDNF–GFR$\alpha$1 complex structure, sucrose octasulfate (SOS), a heparin mimic, was bound to the same region in GFR$\alpha$1, which suggested that the RET and heparin-binding interfaces overlap (Parkash *et al.*, 2008).

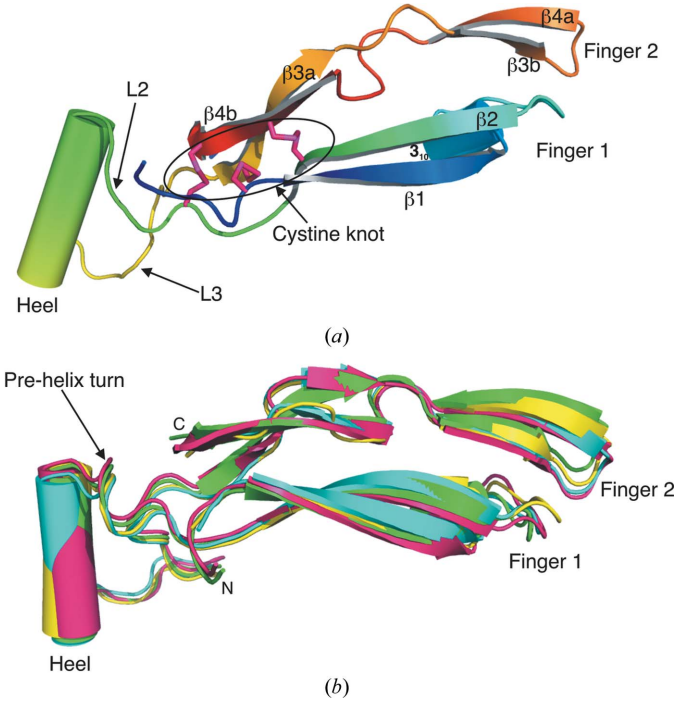


**Figure 1**
The GDNF and ARTN monomer structures. (*a*) The GDNF monomer from the previous GDNF–GFR$\alpha$1 complex (PDB code 2v5e). The structure, coloured from blue to red, consists of two two-$\beta$-strand fingers (finger 1 and 2) and a helical heel. The cystine knot is shown in magenta. (*b*) Structural superposition of selected ARTN monomers. ARTN structures are colour-coded: 2gh0, magenta; 2ask, green; 2gyz, yellow; 2gyr (chains *A* and *B*), cyan. The two other independent ARTN monomers in 2gyr (not shown here) are essentially identical.

**Table 1**
X-ray data-collection and refinement statistics.

Values in parentheses are for the highest resolution shell.

| | |
|---|---|
| Data collection | |
| Resolution range (Å) | 20–2.35 (2.45–2.35) |
| Space group | *C*2 |
| Unit-cell parameters (Å, °) | $a$ = 45.2, $b$ = 84.1, $c$ = 179.2, $\beta$ = 96.1 |
| Wavelength (Å) | 0.933 |
| Molecules per ASU | 2 |
| No. of reflections | |
| Total | 106181 |
| Unique | 27081 |
| Completeness (%) | 97.0 (91.3) |
| $I/\sigma(I)$ | 12.1 (2.95) |
| $R_{merge}$ (%) | 9.0 (43) |
| Refinement | |
| Resolution range (Å) | 20–2.35 |
| Reflections | 25681 |
| $R_{work}$ (%) | 22.5 |
| $R_{free}$ (%) | 28.0 |
| Average $B$ factors (Å$^2$) | |
| Protein (4561 atoms) | 24.5 |
| Solvent (167 atoms) | 21.3 |
| Ethylene glycol (12 atoms) | 35 |
| *N*-Acetylglucosamine (42 atoms) | 48 |
| Sulfate (5 atoms) | 70 |
| R.m.s.d. from ideal values | |
| Bond lengths (Å) | 0.007 |
| Angles (°) | 1.09 |
| Ramachandran plot | |
| Most favoured (%) | 93.5 |
| Additionally allowed (%) | 6.5 |

The structure of the ARTN monomer has an overall fold similar to that of GDNF (Fig. 1), but differs with respect to the hinge angle between the fingers and the heel (Silvian *et al.*, 2006). This difference in the monomer structures is imparted to the GDNF and ARTN homodimers and makes them very dissimilar. We suggested that this

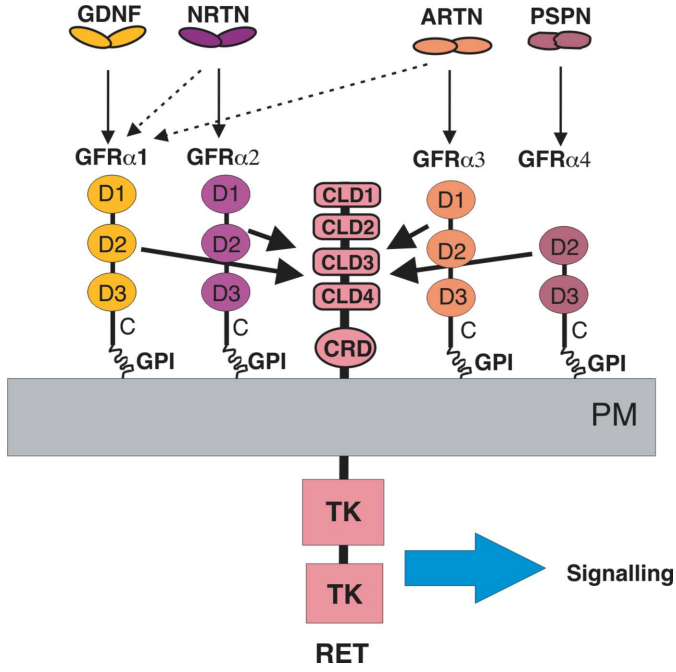


**Figure 2**
The components of RET signalling: GFLs, GFR$\alpha$s and RET. GFLs (GDNF, NRTN, ARTN and PSPN) each bind a specific coreceptor GFR$\alpha$ (GFR$\alpha$1, GFR$\alpha$2, GFR$\alpha$3 and GFR$\alpha$4) and activate the common signalling receptor RET (in light pink). The promiscuity of GFR$\alpha$1 is shown, as it interacts with noncognate GFLs (dotted arrows) apart from PSPN. PM, plasma membrane; TK, tyrosine kinase domain; GPI, glycosylphosphatidyl inositol.

explains why GDNF and ARTN do not signal in the same manner in a mitogen-activated protein kinase (MAPK) assay (Parkash *et al.*, 2008). Although the orientation of the finger domain with respect to the heel varied slightly in previous GDNF structures (Eigenbrot & Gerber, 1997; Parkash *et al.*, 2008), all the ARTN structures solved so far are essentially identical (Fig. 1*b*). Here, we present the structure of another GDNF–GFR$\alpha$1 complex and analyze it to see how it too differs from the previous structures. Our new $GDNF_2$–$GFR\alpha1_2$ complex has a slightly different conformation in the GDNF heel region but is otherwise similar to our first structure. Comparison of 11 different GDNF- and ARTN-containing structures clearly suggests that ARTN is rigid while GDNF is somewhat flexible, but this flexibility is much smaller than the difference between ARTN and GDNF. Our initial conclusion about the possible cause of differential MAPK signalling (Parkash *et al.*, 2008) therefore remains valid.

## 2. Materials and methods

### 2.1. Protein expression and purification

Cloning, expression and purification of GDNF and GFR$\alpha$1 were similar to previously reported methods (Parkash *et al.*, 2008). In brief, rat GFR$\alpha$1 D23C (residues 145–425; UniProt accession No. Q62997) and human GDNF (residues 1–134, excluding the 77-residue preprosequence; UniProt accession No. P39905) were co-expressed in insect cells and purified together using Ni-Sepharose affinity followed by size-exclusion chromatography. We did not include GFR$\alpha$1 D1, as it is not needed for ligand binding (Virtanen *et al.*, 2005). The purified complex was incubated overnight at room temperature with thrombin (10 units per milligram of complex) to remove the His tag.

### 2.2. Crystallization and data collection

The purified complex was concentrated to 3 mg ml$^{-1}$ and the buffer was changed to 10 m*M* HEPES pH 7.5 supplemented with 150 m*M* NaCl, 0.01%(*v*/*v*) P8340 protease-inhibitor cocktail (Sigma) and 0.001% $NaN_3$. The complex was crystallized by sitting-drop vapour diffusion using the Helsinki robot crystallization facility. Crystals of $GDNF_2$–$GFR\alpha1_2$ were obtained in 7 d at 293 K in 15% PEG 4000, 0.15 *M* ammonium sulfate, 0.1 *M* MES buffer pH 6 and were cryoprotected using Paratone-N and frozen at 103 K. The crystal diffracted to 2.35 Å resolution and X-ray diffraction data were collected on an ADSC Q210 CCD detector installed on beamline ID14-1 at the European Synchrotron Radiation Facility (ESRF, France). The data were integrated and scaled in space group *C*2 (Table 1) using the *XDS* and *XSCALE* programs (Kabsch, 1993).

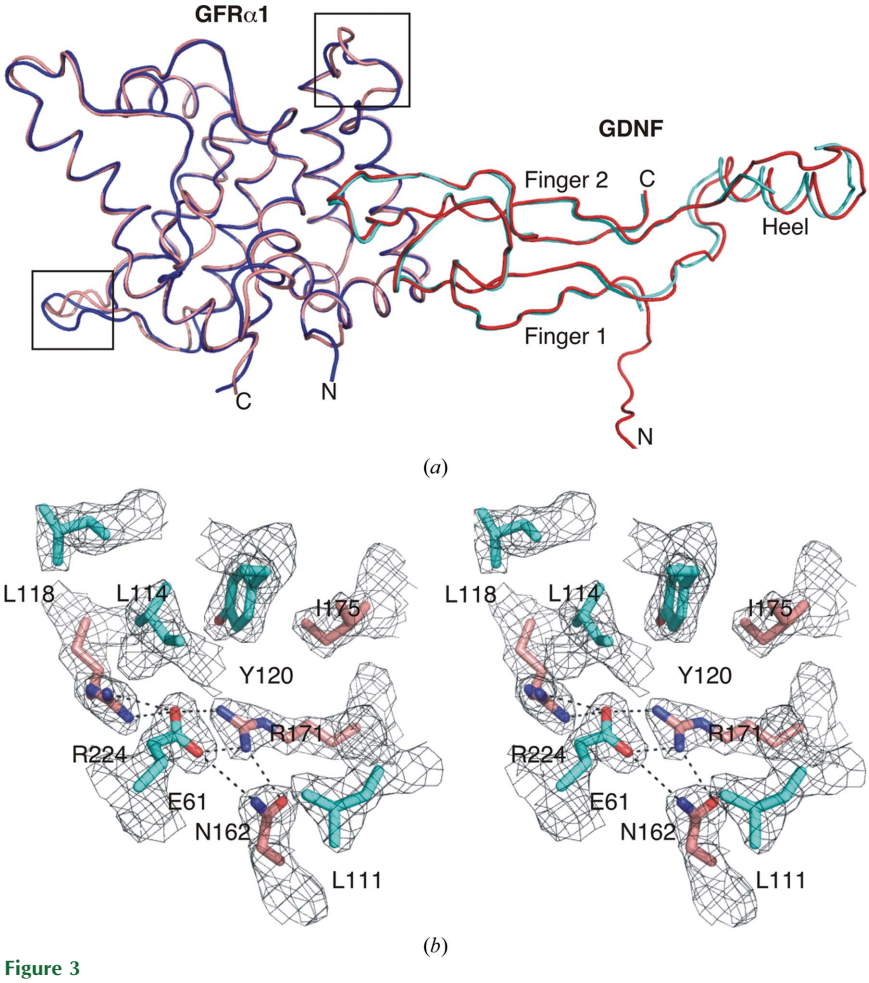


**Figure 3**
The crystal structure of the GDNF–GFR$\alpha$1 complex. (*a*) Heterodimer *AB* is shown in blue (GFR$\alpha$1) and cyan (GDNF), while heterodimer *CD* is shown in light pink and red. The two heterodimers (GDNF–GFR$\alpha$1) are superimposed on each other and the differences are boxed. (*b*) Stereoview of the $2F_o - F_c$ electron-density map contoured at 1.2$\sigma$ at the GDNF–GFR$\alpha$1 interface. The important interface residues surrounding the ion triplet Arg171$^{GFR\alpha1}$–Glu61$^{GDNF}$–Arg224$^{GFR\alpha1}$ are shown with sticks colour-coded as follows: carbon (GFR$\alpha$1), salmon; nitrogen, blue; oxygen, red; carbon (GDNF), cyan.

### 2.3. Structure determination, model building and refinement

The $GDNF_2$–$GFR\alpha1_2$ crystal has different unit-cell parameters from our previous $GDNF_2$–$GFR\alpha1_2$–$SOS_2$ structure, which was crystallized using PEG 8000 (Parkash *et al.*, 2008). The solvent content was 55%, with two heterodimers (GDNF–GFR$\alpha$1; ∼31 kDa) in the asymmetric unit. The structure was solved by molecular replacement using *Phaser* (Collaborative Computational Project, Number 4, 1994). We searched for two GDNF–GFR$\alpha$1 heterodimers using our previous GDNF–GFR$\alpha$1 structure as a model. The results were unambiguous; the initial *Z* scores were 18.8 and 19.5 for the rotation function and 11.3 and 34.6 for the translation function. 5% of reflections (1358) were randomly selected for $R_{free}$ calculation and the remaining data (25 681 reflections) were used in refinement (Table 1). The initial *R* factor after rigid-body refinement was 30% ($R_{free}$ = 34%). We used the program *Coot* (Emsley & Cowtan, 2004) for model building and to add water to peaks above 3.5$\sigma$ in the $F_o - F_c$ difference electron-density map if they had suitable hydrogen-bonding geometry.

The asymmetric unit contains two chains of GFR$\alpha$1 (chain *A*, residues 150–348; chain *C*, residues 150–348) and two chains of GDNF (chain *B*, residues 40–134; chain *D*, residues 32–134). The C-terminus of GFR$\alpha$1, although present in the expressed protein, appears to have been proteolysed during purification and crystallization. The N-terminal region (residues 1–39 in chain *B* and 1–31 in chain *D*) of GDNF was disordered. The GDNF heel (residues 78–89) and the two GFR$\alpha$1 loop regions in D2 (residues 179–188) and D3 (residues 267–278) were in a

**Table 2**
Structural alignment table.

The structures used in the alignment are GDNF–GFRα1 from this paper (PDB code 3fub; chains *AB* and *CD*), the original GDNF–GFRα1 (PDB code 2v5e; Parkash *et al.*, 2008), ARTN–GFRα3 (PDB code 2gh0; Wang *et al.*, 2006) and GDNF (PDB code 1agq; Eigenbrot & Gerber, 1997).

| Aligned | GFL fingers, r.m.s.d. for 57 $C^{\alpha}$ (Å) | GFL monomer, r.m.s.d for 85 $C^{\alpha}$ (Å) | GFL dimer, r.m.s.d. for 180 $C^{\alpha}$ (Å) | Heterodimer, r.m.s.d. for 280 $C^{\alpha}$ (Å) | Heterotetramer, r.m.s.d. for 560 $C^{\alpha}$ (Å) |
|---|---|---|---|---|---|
| 3fub†; *AB versus CD* | 0.05 | 0.25 | 0.55 | 0.62 | 1.0 |
| 1agq; *AB versus CD* | 0.3 | 1.5 | 2.6 | — | — |
| 2v5e *versus* 3fub‡ | 0.33 | 1.31 | 1.73 | 1.92 | 3.4 |
| 1agq *versus* 3fub‡§ | 0.68, 0.53 | 1.28, 1.37 | 1.8, 1.9 | — | — |
| 2gh0 *versus* 3fub‡ | 1.56 | 2.9 | 4.5 | 3.7 | — |

† Two heterodimers in the asymmetric unit. ‡ Chains *A* and *B* are used for superposition. § The first value corresponds to alignment of chain *A* in 1agq and the second to alignment of chain *C*.

different conformation than in our original structure (PDB code 2v5e; Parkash *et al.*, 2008) and thus were deleted and rebuilt manually using *Coot*. The D3 loop conformation in chain *A* was almost identical to the corresponding loop conformation in the GFRα1 D3 structure (PDB code 1q8d; Leppänen *et al.*, 2004), so it was used to build the loop. Residues 93–95 in chain *B* were disordered. We refined the structure using *REFMAC*5 (Murshudov *et al.*, 1999) to a final *R* factor of 22.5% ($R_{\rm free}$ = 28%). The model was validated using *MolProbity* (Davis *et al.*, 2007) and *Coot* (Emsley & Cowtan, 2004). More than 93% of the residues are in the favourable regions of the Ramachandran plot (Table 1).

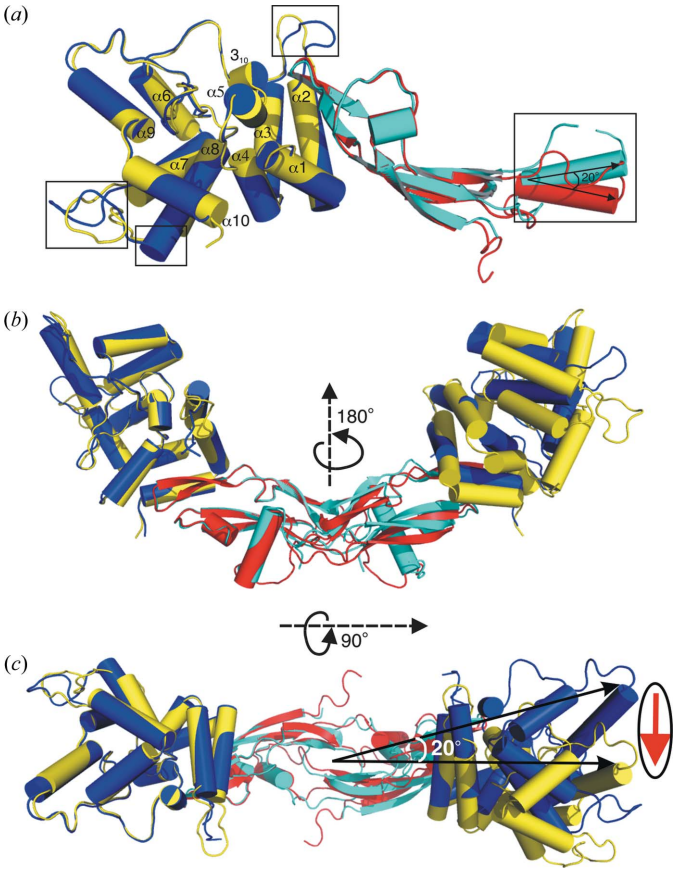


**Figure 4**
Comparison with previous ligand–coreceptor structures. (*a*) Heterodimer superposition of GDNF–GFRα1 structures. 2v5e (GDNF, red; GFRα1, yellow) was superimposed on 3fub (GDNF, cyan; GFRα1, blue). The GFRα1s were superimposed. The differences in the loop (GFRα1) and heel (GDNF) regions are marked with boxes. The same colour coding is used in (*b*) and (*c*), which show the heterotetramer superposition of the $GDNF_2$–$GFR\alpha1_2$ structure. The left-hand heterodimer was superimposed to show the differences in the right-hand heterodimer. The twofold axis in the two heterotetramers is thus in a slightly different position in each structure; the one shown is for 3fub. The GDNF bend angle is essentially the same in both structures. (*c*) is rotated 90° from (*b*) about the horizontal axis. The red arrow represents the direction of motion between the two right-hand GFRα1s.

### 2.4. The bend-angle calculations and structural superposition

Previously, the hinge angle between the heel and fingers of the monomer structure was measured to compare the GDNF and ARTN monomer structures (Silvian *et al.*, 2006). To describe the difference between the GFLs and their complexes, we characterized each by a GFL intermonomer bend angle. This was calculated as the Glu61 $C^{\alpha}$—Cys101 $S^{\gamma}$—Glu61 $C^{\alpha\prime}$ angle (GDNF numbering). We chose Glu61 because it forms the primary interaction at the co-receptor-binding interface. The structural superposition and the bend-angle measurements were performed using *PyMOL* (DeLano, 2002).

## 3. Results and discussion

### 3.1. Asymmetric unit

The asymmetric unit in the crystal contains two GDNF–GFRα1 heterodimer complexes related by twofold noncrystallographic symmetry (NCS). Each heterodimer consists of GFRα1 containing two domains, D2 and D3, and a GDNF monomer. There are thus two independent tetramers in the unit cell, each formed around one of the unique crystallographic twofold axes in space group *C*2. A region of residues within GFRα1 D23 mediates the contacts between the heterodimers. The GDNF complex was not deglycosylated, unlike previously (Parkash *et al.*, 2008), and therefore electron density for *N*-acetylglucosamine (NAG) molecules attached to the N-terminus of GDNF was visible. We could model two NAG residues attached to GDNF Asn49 in one heterodimer (chains *C* and *D*) and one in the other heterodimer (chains *A* and *B*).

The heterodimer superposition gave a root-mean-square deviation (r.m.s.d.) of 0.6 Å for 280 $C^{\alpha}$-atom positions (Table 2); the structures are thus almost identical (Fig. 3*a*) except for the GFRα1 loops, which differ owing to crystal packing. In the following, we therefore discuss only chains *A* and *B* of the two GDNF–GFRα1 heterodimers present in the asymmetric unit. The electron-density map (Fig. 3*b*) was good throughout the structure except for the loops.

### 3.2. Structural comparison

Our previous study described the differences between the $GDNF_2$–$GFR\alpha1_2$ (PDB code 2v5e) and $ARTN_2$–$GFR\alpha3_2$ (PDB code 2gh0) structures, which are essentially imparted by the structural dissimilarity between GDNF and ARTN (Parkash *et al.*, 2008). The $GDNF_2$–$GFR\alpha1_2$ complex (PDB code 3fub) crystallized in a different

crystal form to 2v5e. This allowed us to study the causes of variability in GFL–GFR$\alpha$ complexes and to examine whether these arise from crystal contacts.

Unsurprisingly, the ligand–coreceptor binding interfaces in 2v5e and 3fub are identical and are composed of the ion-triplet $Arg171^{GFR\alpha1}$–$Glu61^{GDNF}$–$Arg224^{GFR\alpha1}$, which is surrounded by $Asn162^{GFR\alpha1}$, $Ile175^{GFR\alpha1}$, $Leu114^{GDNF}$ and $Tyr120^{GDNF}$ (Fig. 3*b*). The r.m.s.d. between the two GDNF–GFR$\alpha$1 heterodimers is 1.9 Å for 280 $C^{\alpha}$ atoms (Fig. 4*a*; Table 2). The GFR$\alpha$1 D23 structures are identical except that loop 279–282 forms an $\alpha$-helical turn, thus extending the N-terminus of helix $\alpha$8 (Fig. 4*a*).

Both 2v5e and our new structure 3fub share one crystal contact: the GDNF finger 1 loop (residues Thr51 and Glu58) and the heel (residues Lys81, Asn85, Arg88, Asn89 and Arg91) interact with the neighbouring GFR$\alpha$1 D23 (residues Asp201, Tyr254, Arg259, Asp262, Asp284 and Leu287). This is the same region where sucrose octasulfate (bound to GFR$\alpha$1 D2) in 2v5e interacted with the symmetry-related GDNF heel (Parkash *et al.*, 2008). Likewise, the disaccharide (NAG-NAG) attached to GDNF Asn49 in 3fub (chain *D*) is in proximity to the SOS-binding region (Asn188, Lys191, Lys194, Arg197 and Gln198) in GFR$\alpha$1, which probably interacts with it. [The presence of this interaction lends further credence to our speculation (Parkash *et al.*, 2008) that heparin-mediated GDNF–GFR$\alpha$1 interactions explain how they act as adhesins during synapse formation (Ledda *et al.*, 2007).] In 3fub, however, each GFR$\alpha$1 forms additional contacts with a noncrystallographically related GFR$\alpha$1. These interactions are between the Ser273–Glu280 region on one monomer and the Val186–Lys191 region on the other. There are four such symmetry-related interactions. The crystal packing in 3fub and 2v5e thus differs and therefore the similarities in the structures probably do not arise from crystal packing.

The largest difference between 2v5e and 3fub is in the GDNF (Fig. 4). In the heterodimer superposition (Table 2), the GDNF heel in 3fub was rotated by about 20° with respect to 2v5e (Fig. 4*a*), but the bend angle in the GDNFs is essentially the same in both (Fig. 4*b*): 158° in 3fub (Fig. 5*a*) and 160° in 2v5e. However, there is a small change when the complex is viewed down the twofold axis; the right-hand GDNF–GFR$\alpha$1 heterodimer is rotated by about 20° (Fig. 4*c*). Nonetheless, the separation between the two putative RET-binding surfaces, such as the extreme end Glu323, is 116 Å, which is almost identical to that in the previous structure (Parkash *et al.*, 2008). Thus, the structural changes caused by the apparent ligand flexibility in the GDNF complex do not substantially affect the RET-binding surface.

However, the same superposition using the $ARTN_2$–$GFR\alpha3_2$ structure gives a very different result (Fig. 5*c*). When the left-hand heterodimers (3fub and 2gh0) are superimposed (Table 2), the right-hand heterodimers make an angle of about 48° with each other (Fig. 5). This large-scale structural change owing to the difference in the GFL bend angle is the same as in 2v5e (Parkash *et al.*, 2008). The new complex structure thus confirms our earlier proposal: variations

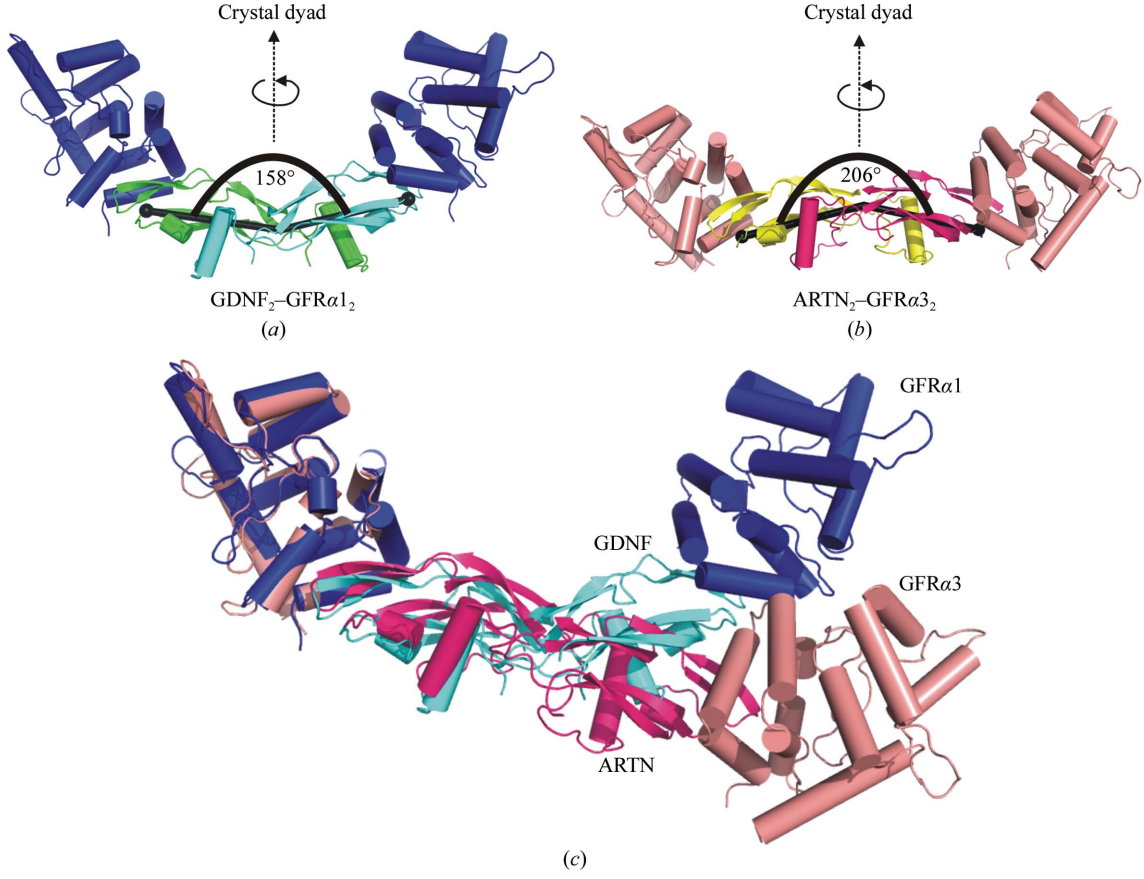


**Figure 5**
GFL bend angle and comparison of the $GDNF_2$–$GFR\alpha1_2$ and $ARTN_2$–$GFR\alpha3_2$ structures. (*a*) The bend angle for the GDNF complex structure (PDB code 3fub). Using *PyMOL* (DeLano, 2002), the bend angle is measured between two finger domains on both monomers (in black spheres) from the intermonomer disulfide bridge (see §2). The monomers in the GDNF homodimer are in cyan and green and the GFR$\alpha$1s are in blue. (*b*) The bend angle for the ARTN complex structure. The ARTN homodimer is shown in magenta and yellow and the GFR$\alpha$3s are in salmon. (*c*) Heterotetramer superposition of the $ARTN_2$–$GFR\alpha3_2$ (PDB code 2gh0) and $GDNF_2$–$GFR\alpha1_2$ (PDB code 3fub) structures. The left-hand heterodimers were superimposed as in Fig. 4(*b*). The GDNF homodimer is shown in cyan and ARTN in magenta. GFR$\alpha$1 and GFR$\alpha$3s are shown in blue and salmon as in (*a*) and (*b*).

in bend angle may explain why GDNF–GFR$\alpha$1 causes faster activation of MAPK through RET than ARTN–GFR$\alpha$3 does (Parkash *et al.*, 2008).

In summary: the minor structural variations in GDNF do not affect the overall geometry of the complex (Fig. 4), but the larger difference between GDNF and ARTN does (Fig. 5). The larger difference is not a crystal artifact: all GDNF and ARTN structures studied to date (Eigenbrot & Gerber, 1997; Silvian *et al.*, 2006; Wang *et al.*, 2006; Parkash *et al.*, 2008) show this large difference (Fig. 6). In addition, the 11 unique GDNF and ARTN structures now allow a meaningful discussion of GFL flexibility. All the ARTN structures have a bend angle of 201–206° and superimpose on each other with r.m.s.d.s of about 1 Å, while the GDNF structures are more bent and appear to be more flexible, with bend angles of 146–168°, and superimpose on each other with larger r.m.s.d.s of 1.7–2.6 Å (Table 2). Why is this so?

### 3.3. Shared basis for GFL variation

Previous structural studies showed the differences in the hinge angles between the heel and the fingers in the GDNF and ARTN monomer structures (Silvian *et al.*, 2006). The estimate of hinge angle for each GDNF monomer in 1agq was about 90° and was 83° for the ARTN monomer (code PDB code 2ask; Silvian *et al.*, 2006). The difference in the monomer hinge angle (or homodimer bend angle) and the increased flexibility appear to have the same cause. The GDNF fingers are less curved (Silvian *et al.*, 2006; Fig. 1) than the ARTN fingers. Consequently, the GDNF homodimer buries about 800 Å$^2$ less surface area (Fraternali & Cavallo, 2002) than the ARTN homodimer. The change in curvature also affects the heel–finger hinge angle and thus the intermonomer bend angle.

The molecular basis for this rests in specific side-chain interactions at the homodimer interface. At the interface, the ligand heel in one monomer packs against residues from the finger domain in the other monomer. The most significant difference is Ile82$^{GDNF}\rightarrow$Ser$^{ARTN}$ in the heel, accompanied by the complementary His126$^{GDNF}\rightarrow$Leu$^{ARTN}$ mutation in the finger domain of the other monomer. In GDNF, the bulkier Ile82 pushes His126 back, which in turn pushes on Leu111 in $\beta$3b (Fig. 7*a*). Ser82$^{ARTN}$ and Val111$^{ARTN}$ (GDNF numbering) are smaller than their GDNF counterparts and the ARTN Ser82–Leu126–Val111 interactions thus bring the fingers closer to the heel (Fig. 7*a*), as does the Leu48$^{GDNF}\rightarrow$Val$^{ARTN}$ at finger 1. All these changes cause the ARTN fingers to be more curved than the GDNF fingers, thus bringing the fingers closer to the heel (Fig. 7*a*) and increasing the bend angle between the fingers. The sequence alignment suggests that the homodimer interface in NRTN will be similar to that of ARTN, not GNDF, as three of the four residues mentioned above show the same changes (Fig. 8). The only position that differs is Ile82$^{GDNF}$, which is Ser in ARTN (see above) and Gly in NRTN; this should increase, not decrease, the level of curvature. We therefore predict that NRTN will be rigid and essentially flat like ARTN. This also implies that NRTN will show ARTN-like, not GDNF-like, MAPK activation.

Finally, the pre-helix and the post-helix loops also appear to influence the bend angle. L3 in GDNF contains Arg (Fig. 8) and is disordered or has high *B* factors in all of the GDNF-containing crystal structures (Table 3). Such apparent flexibility would allow the fingers and the heel to move independently. Conversely, L3 is more ordered in all six ARTN structures (Silvian *et al.*, 2006; Wang *et al.*, 2006; Fig. 1*b*), possibly because of the proline residues in the loop (Fig. 8). The reverse seems to be true in the pre-helix L2 region. Here, the positively charged $^{73}$RRARS$^{77}$ in ARTN forms a $3_{10}$-helix, while the GDNF $^{73}$DAAET$^{77}$ does not (Fig. 1). This change affects the relative orientation of finger 1 with respect to the heel and thus the hinge angle.

**Table 3**
Missing residues or residues with high mobility in loop L3 in GDNF structures.

| PDB code | Average *B* factor (Å$^2$) (resolution) | Chain | Missing residues | *B* factors >40 Å$^2$ | Reference |
|---|---|---|---|---|---|
| 2v5e | 27 (2.35 Å) | *B* | — | 92–97 | Parkash *et al.* (2008) |
| 1agq | 33 (1.9 Å) | *A* | 92–97 | — | Eigenbrot & Gerber (1997) |
| 1agq | 33 (1.9 Å) | *B* | 96–97 | 94–95 | Eigenbrot & Gerber (1997) |
| 1agq | 33 (1.9 Å) | *C* | 94–97 | 92–93, 98–99 | Eigenbrot & Gerber (1997) |
| 1agq | 33 (1.9 Å) | *D* | — | 94–96 | Eigenbrot & Gerber (1997) |
| 3fub | 24 (2.35 Å) | *B* | 93–95 | 92, 96–100 | This study |
| 3fub | 24 (2.35 Å) | *D* | — | 91–100 | This study |

### 3.4. An extended model for differential signalling

The coreceptor-binding residues of GDNF, NRTN, ARTN and PSPN centred around Glu61 (GDNF numbering) are similar and so differences between the ligands presumably reside outside the

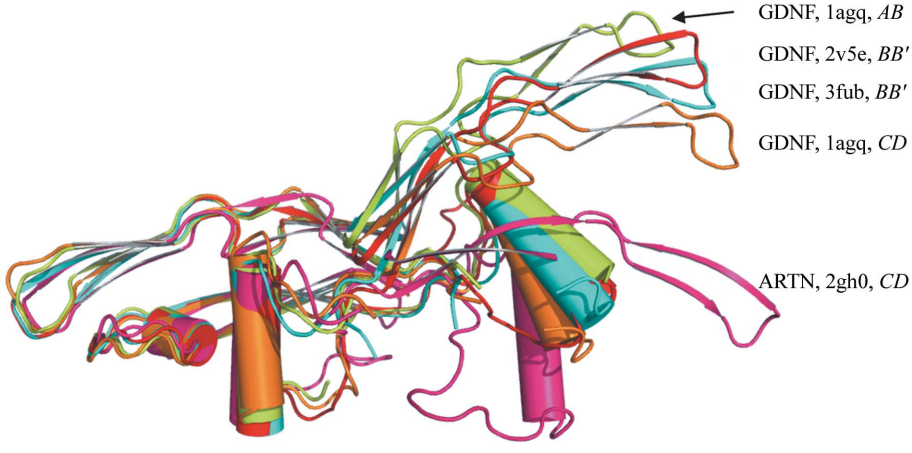


**Figure 6**
Superposition of selected GFL homodimers. Structural superposition of ARTN and four GDNF structures. The monomer finger domains were superimposed. The ARTN structure is in magenta (PDB code 2gh0). Unbound GDNF (PDB code 1agq; Eigenbrot & Gerber, 1997) exists in two conformations: chain *AB* (in lemon) and chain *CD* (in orange). GDNF from 2v5e is in red and that from 3fub is in cyan. Finger 1 in the right-hand monomer is not shown for clarity. Only one of the five independent ARTN structures is shown as they are almost identical (see Fig. 1*b*).

interface, as we proposed previously (Parkash *et al.*, 2008). It is intriguing, however, that PSPN shows no sign of crosstalk with GFR$\alpha$1–RET even *in vitro* (Airaksinen & Saarma, 2002), unlike NRTN and ARTN. Detailed structural analysis may provide an explanation.

Functional mapping of GDNF, NRTN and ARTN showed three critical regions (Fig. 8) for GFR$\alpha$1–RET activation in RET-3T3 cells (Baloh *et al.*, 2000): region I (residues 73–80), region II (residues 103–110) and region III (residues 120–127) (GDNF numbering). Of these, regions I and II are not involved in coreceptor binding and so these must have a more direct effect on RET activation. There are two possibilities: either regions I and II from GDNF, NRTN and ARTN, but not from PSPN, may be in contact with RET or regions I and II may affect the homodimeric structural conformation of the GFLs. Region I is composed of the pre-helix segment and the sequence is essentially not conserved. Region II within $\beta$-strand 3 in PSPN is very similar to that of ARTN. Thus, regions I and II are less likely to interact with RET, if we assume that the same surface in RET interacts with the coreceptors, and so the same surface needs to be present on the coreceptors.

It thus seems more likely that these regions affect the structure of the homodimer. We found that Asp80 (region I) and Arg103 (region II) are the only two residues that are conserved in GDNF, NRTN and ARTN but not in all PSPNs (Fig. 8). Intriguingly, the GDNF and ARTN structures showed a unique intermonomer ion pair formed between Asp80 and Arg103 at the homodimer interface (Figs. 7*b* and 7*c*). This interaction appears to be essential in locking the movement of the heel, as one side of the heel is buried but the other side is exposed to solvent. This may explain why regions I and II of GDNF/NRTN/ARTN are required to allow mouse PSPN chimeras to signal through GFR$\alpha$1 (Baloh *et al.*, 2000). The lack of this ion pair may lead to a difference in the structure of the PSPN homodimer. This could affect how the PSPN–GFR$\alpha$4 complex activates RET tyrosine kinase and thus explain the lack of PSPN–GFR$\alpha$1 crosstalk (Airaksinen *et al.*, 1999).

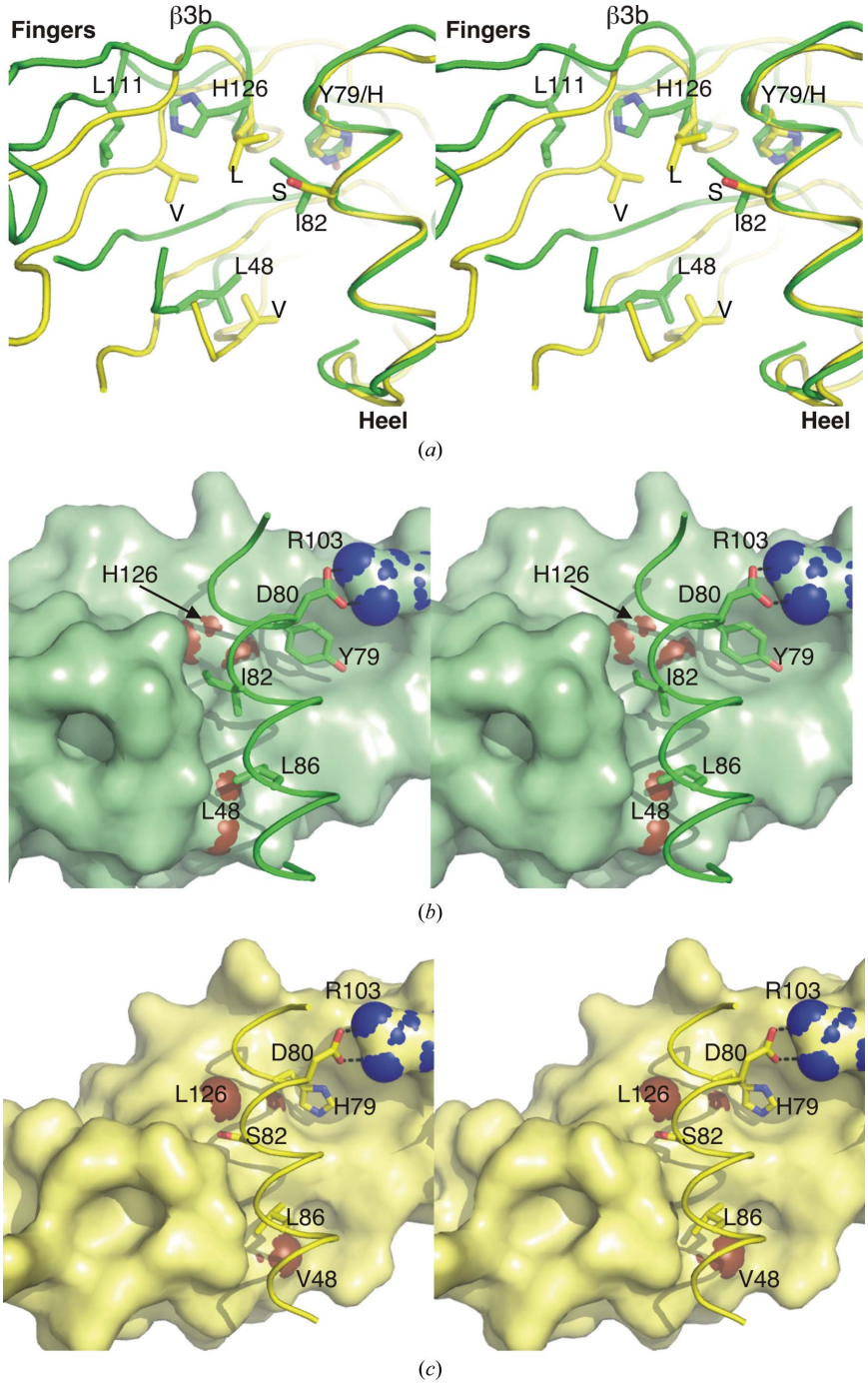


**Figure 7**
Stereoviews of the GDNF and ARTN homodimer interface. (*a*) Interaction between the finger domains and the heel at the GDNF and ARTN homodimer interface. The heel regions of the GDNF and ARTN structures are superimposed to show the differences. Finger 1 residues 50–61 are not shown for clarity. The cartoon loop structure of GDNF is in green, while that of ARTN is in yellow. The buried residues at the homodimer interface are shown in sticks: carbon, green (GDNF) and yellow (ARTN); oxygen, red; nitrogen, blue. Only GDNF residues are numbered. (*b*) Interaction of the GDNF heel with the finger domain and the intermonomer ion pair. One monomer is in surface representation (in pale green), while the heel of the other monomer is shown in green. The important interface residues that are not conserved among GFLs are shown as a brown surface for the bottom monomer and as sticks for the heel. The intermonomer ion pair between Asp80 and Arg103 is also shown. (*c*) The ARTN homodimer as in (*b*). The finger domain is shown as a pale yellow surface and heel is shown as a yellow loop.

## 4. Conclusions

Our second crystal structure of the GDNF–GFR$\alpha$1 complex provides further evidence that GFL signalling through RET is determined by the bend angle in the GFL. Our detailed analysis of the 11 GFL structures obtained to date, both alone and complexed with GFR$\alpha$s, also indicates that the bend angle and apparent flexibility differences are intrinsic to the GFLs. They do not appear to arise from crystal-packing artifacts. We have been able to explain why GDNF is both more bent and more flexible than ARTN (and probably NRTN). Finally, our structural data suggest that Asp80–Arg103 is important in determining RET activation through GFR$\alpha$1.

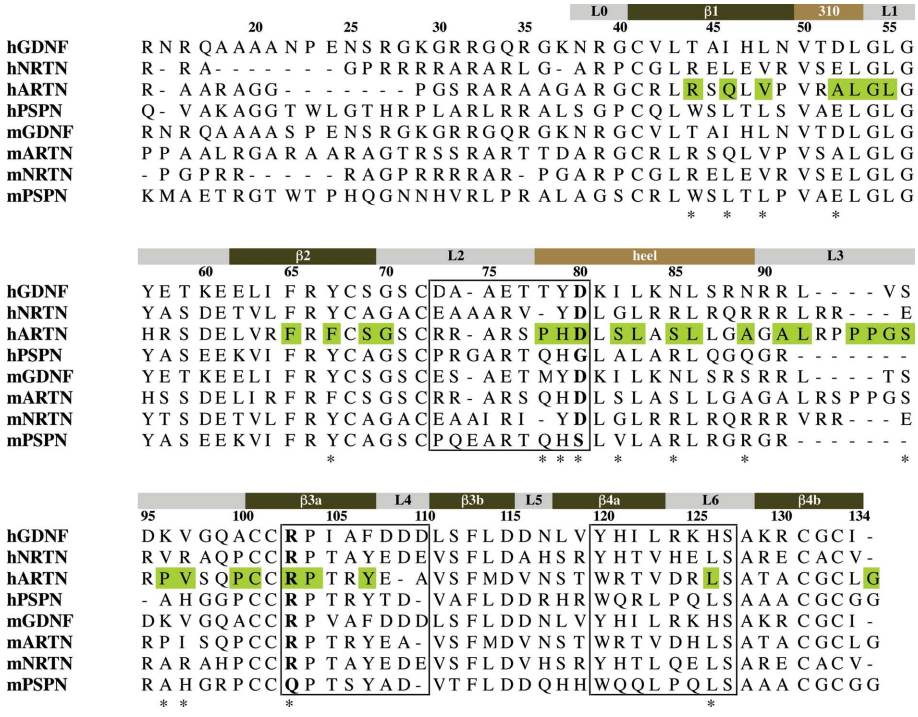


**Figure 8**
Sequence alignment between GFLs. Based on the GDNF structure, human and mouse GFL sequences are aligned. The secondary structure is shown at the top together with the numbering according to human GDNF. GDNF $\beta$-strands 3 and 4 are split because of the insertion of loops L4 and L6. GDNF fingers 1 and 2 are composed of $\beta$-strands 1 and 2 and $\beta$-strands 3 and 4, respectively, as described previously (Eigenbrot & Gerber, 1997). The residues in the larger ARTN interface region have a green background. The residues Asn80 and Arg103 forming an ion pair in the GDNF and ARTN structures are shown in bold. The nonconserved buried residues are marked with an asterisk under the sequence alignment. Three critical segments for GFR$\alpha$1–RET activation identified in previous studies (Baloh *et al.*, 2000) are boxed.

This work thus further helps to define the structural determinants of RET activation.

This work was supported by Academy of Finland grants 1111771 and 1114752 to AG, a VGSB fellowship to VP and the Sigrid Juselius Foundation. We thank Seija Mäki and the Helsinki crystallization facility for skilled technical help and Dr Veli-Matti Leppänen for providing the high-titre baculovirus virus stock. We thank Esko Oksanen and Drs Chiara Bruckmann and Andrzej Lyskowski for helpful discussions. We acknowledge the European Synchrotron Radiation Facility for provision of synchrotron-radiation resources and thank Dr Xavier Thibault for assistance in using beamline ID14-EH1. Beam time was made available under the European Union Improving Human Potential Programme (Access to Research Infrastructures) at the ESRF under contract No. HPRI-CT-1999-00022.

## References

Airaksinen, M. S. & Saarma, M. (2002). *Nature Rev. Neurosci.* **3**, 383–394.
Airaksinen, M. S., Titievsky, A. & Saarma, M. (1999). *Mol. Cell. Neurosci.* **13**, 313–325.
Baloh, R. H., Tansey, M. G., Johnson, E. M. Jr & Milbrandt, J. (2000). *J. Biol. Chem.* **275**, 3412–3420.
Baloh, R. H., Tansey, M. G., Lampe, P. A., Fahrner, T. J., Enomoto, H., Simburger, K. S., Leitner, M. L., Araki, T., Johnson, E. M. Jr & Milbrandt, J. (1998). *Neuron*, **21**, 1291–1302.
Collaborative Computational Project, Number 4 (1994). *Acta Cryst.* D**50**, 760–763.
Davis, I. W., Leaver-Fay, A., Chen, V. B., Block, J. N., Kapral, G. J., Wang, X., Murray, L. W., Arendall, W. B. III, Snoeyink, J., Richardson, J. S. & Richardson, D. C. (2007). *Nucleic Acids Res.* **35**, W375–W383.
DeLano, W. L. (2002). *The PyMOL Molecular Graphics System.* DeLano Scientific, Palo Alto, California, USA.
Eigenbrot, C. & Gerber, N. (1997). *Nature Struct. Biol.* **4**, 435–438.
Eketjäll, S., Fainzilber, M., Murray-Rust, J. & Ibáñez, C. F. (1999). *EMBO J.* **18**, 5901–5910.
Emsley, P. & Cowtan, K. (2004). *Acta Cryst.* D**60**, 2126–2132.
Fraternali, F. & Cavallo, L. (2002). *Nucleic Acids Res.* **30**, 2950–2960.
Kabsch, W. (1993). *J. Appl. Cryst.* **26**, 795–800.
Kotzbauer, P. T., Lampe, P. A., Heuckeroth, R. O., Golden, J. P., Creedon, D. J., Johnson, E. M. Jr & Milbrandt, J. (1996). *Nature (London)*, **384**, 467–470.
Ledda, F., Paratcha, G., Sandoval-Guzmán, T. & Ibáñez, C. F. (2007). *Nature Neurosci.* **10**, 293–300.
Leppänen, V.-M., Bespalov, M. M., Runeberg-Roos, P., Puurand, Ü., Merits, A., Saarma, M. & Goldman, A. (2004). *EMBO J.* **23**, 1452–1462.
Lindahl, M., Poteryaev, D., Yu, L., Arumäe, U., Timmusk, T., Bongarzone, I., Aiello, A., Pierotti, M. A., Airaksinen, M. S. & Saarma, M. (2001). *J. Biol. Chem.* **276**, 9344–9351.
Milbrandt, J. *et al.* (1998). *Neuron*, **20**, 245–253.
Murshudov, G. N., Vagin, A. A., Lebedev, A., Wilson, K. S. & Dodson, E. J. (1999). *Acta Cryst.* D**55**, 247–255.
Parkash, V., Leppänen, V.-M., Virtanen, H., Jurvansuu, J.-M., Bespalov, M. M., Sidorova, Y. A., Runeberg-Roos, P., Saarma, M. & Goldman, A. (2008). *J. Biol. Chem.* **283**, 35164–35172.
Scott, R. P. & Ibáñez, C. F. (2001). *J. Biol. Chem.* **276**, 1450–1458.
Silvian, L., Jin, P., Carmillo, P., Boriack-Sjodin, P. A., Pelletier, C., Rushe, M., Gong, B., Sah, D., Pepinsky, B. & Rossomando, A. (2006). *Biochemistry*, **45**, 6801–6812.
Virtanen, H., Yang, J., Bespalov, M. M., Hiltunen, J. O., Leppänen, V.-M., Kalkkinen, N., Goldman, A., Saarma, M. & Runeberg-Roos, P. (2005). *Biochem. J.* **387**, 817–824.
Wang, X., Baloh, R. H., Milbrandt, J. & Garcia, K. C. (2006). *Structure*, **14**, 1083–1092.